## SPECIAL ISSUE ARTICLE



WILEY

# A new method for scaling inlet flow waveform in hemodynamic analysis of aortic dissection

Kaihong Wang<sup>1</sup> | Chlöe H. Armour<sup>1,2</sup> | Baolei Guo<sup>3</sup> | Zhihui Dong<sup>3</sup> Xiao Yun Xu<sup>1</sup>

#### Correspondence

Xiao Yun Xu, Department of Chemical Engineering, Imperial College London, South Kensington Campus, London SW7 2AZ, UK.

Email: yun.xu@imperial.ac.uk

Baolei Guo and Zhihui Dong, Department of Vascular Surgery, Zhongshan Hospital, Fudan University, Shanghai, China. Email: guo.baolei@zs-hospital.sh.cn and dong.zhihui@zs-hospital.sh.cn

### **Funding information**

National Natural Science Foundation of China, Grant/Award Number: 81770508; Natural Science Foundation Project of Fujian Province, Grant/Award Number: 2023J011687; Science and Technology Commission of Shanghai Municipality, Grant/Award Number: 21410710500; Shanghai Municipal Health Commission's Health Youth Talent Training Program, Grant/Award Number: 2022YQ13; Clinical Medicine Innovation Fund of Fudan Zhangjiang Institute, Grant/Award Number: KP7202116; Royal Society, UK, Grant/Award Number: IE161052; Imperial College London BHF Centre of Research Excellence, Grant/Award Number: RE/18/ 4/34215

#### **Abstract**

Computational fluid dynamics (CFD) simulations have shown great potentials in cardiovascular disease diagnosis and postoperative assessment. Patient-specific and well-tuned boundary conditions are key to obtaining accurate and reliable hemodynamic results. However, CFD simulations are usually performed under non-patient-specific flow conditions due to the absence of in vivo flow and pressure measurements. This study proposes a new method to overcome this challenge by tuning inlet boundary conditions using data extracted from electrocardiogram (ECG). Five patient-specific geometric models of type B aortic dissection were reconstructed from computed tomography (CT) images. Other available data included stoke volume (SV), ECG, and 4D-flow magnetic resonance imaging (MRI). ECG waveforms were processed to extract patient-specific systole to diastole ratio (SDR). Inlet boundary conditions were defined based on a generic aortic flow waveform tuned using (1) SV only, and (2) with ECG and SV (ECG + SV). 4D-flow MRI derived inlet boundary conditions were also used in patient-specific simulations to provide the gold standard for comparison and validation. Simulations using inlet flow waveform tuned with ECG + SV not only successfully reproduced flow distributions in the descending aorta but also provided accurate prediction of timeaveraged wall shear stress (TAWSS) in the primary entry tear (PET) and abdominal regions, as well as maximum pressure difference,  $\Delta P_{\text{max}}$ , from the aortic root to the distal false lumen. Compared with simulations with inlet waveform tuned with SV alone, using ECG + SV in the tuning method significantly reduced the error in false lumen ejection fraction at the PET (from 149.1% to 6.2%), reduced errors in TAWSS at the PET (from 54.1% to 5.7%) and in the abdominal region (from 61.3% to 11.1%), and improved  $\Delta P_{\text{max}}$  prediction (from 283.1% to 18.8%) However, neither of these inlet waveforms could be

This is an open access article under the terms of the Creative Commons Attribution License, which permits use, distribution and reproduction in any medium, provided the original work is properly cited.

<sup>&</sup>lt;sup>1</sup>Department of Chemical Engineering, Imperial College London, London, UK

<sup>&</sup>lt;sup>2</sup>National Heart and Lung Institute, Imperial College London, London, UK

<sup>&</sup>lt;sup>3</sup>Department of Vascular Surgery, Zhongshan Hospital, Fudan University, Shanghai, China

<sup>© 2024</sup> The Author(s). International Journal for Numerical Methods in Biomedical Engineering published by John Wiley & Sons Ltd.

2040/947, 2024, 9, Downloaded from https://onlinelibtrary.wiley.com/doi/10.1002/cmm.3885 by Imperial College London, Wiley Online Library on [2810/2025]. See the Terms and Conditions (https://onlinelibtrary.wiley.com/terms-and-conditions) on Wiley Online Library for rules of use; OA articles are governed by the applicable Creative Commons License

used for accurate prediction of TAWSS in the ascending aorta. This study demonstrates the importance of SDR in tailoring inlet flow waveforms for patient-specific hemodynamic simulations. A well-tuned flow waveform is essential for ensuring that the simulation results are patient-specific, thereby enhancing the confidence and fidelity of computational tools in future clinical applications.

#### **KEYWORDS**

aortic dissection, computational fluid dynamics, electrocardiogram, flow waveform, wall shear stress

## 1 | INTRODUCTION

Computational fluid dynamics (CFD) simulations have become a robust and widely adopted tool in assessing hemodynamics in the aorta. Near-wall hemodynamic parameters, such as wall shear stress (WSS) and relative residence time (RRT) are usually quantified to investigate their association with aortic disease progressions. <sup>1-7</sup> Low WSS has been found to promote atherosclerosis from both in-vivo and computational studies, <sup>8-10</sup> and regions with extremely low WSS and long RRT are more likely to induce false lumen (FL) thrombosis in aortic dissection. <sup>11-14</sup> On the other hand, high WSS has been found to be a potential risk factor in the development of stent graft-induced new entry (SINE) tears in a recent study. <sup>6</sup> In addition, flow characteristics such as retrograde flow in the descending aorta have been suggested as a risk factor for aortic enlargement. <sup>15-17</sup> Low relative pressure difference between the aortic root and FL is also an indicator for FL expansion. <sup>17</sup> These studies demonstrate the great potential of CFD in answering clinical questions and being used as a tool to assist clinical decision making. Therefore, the accuracy of simulations is crucial to ensure the reliability of CFD assessments. For flow in the aorta, boundary conditions play an important role in obtaining accurate hemodynamic results. Patient-specific information such as flow and Doppler-wire pressure measurements are desired for such simulations, and well-tuned physiological boundary conditions should be applied at both inlet and outlets.

Several studies have investigated the effects of different boundary conditions on simulation results. At model inlets, non-patient-specific waveforms significantly affect the distribution and magnitude of hemodynamic results, particularly WSS. <sup>18,19</sup> A 25% reduction of stroke volume can result in errors of up to 35% and 28% in WSS and velocity. <sup>19</sup> Patient-specific spatiotemporal inlet velocity profiles extracted from 4-dimensional magnetic resonance imaging (4D-flow MRI) has the best performance in capturing the hemodynamics in the aorta compared with flat and parabolic profiles, especially in the ascending aorta. <sup>18–20</sup> Even with spatiotemporally distributed inlet velocity profiles, difference in the spatial distribution, such as the shape of the truncated cone, can greatly impact WSS and velocity distributions. <sup>21</sup> At model outlets, 3-element Windkessel model (3EWM) with well-tuned parameters is recommended as a reliable boundary condition to represent hemodynamic resistance and vessel compliance. <sup>22–25</sup> A workflow presented by Pirola et al., <sup>25</sup> which utilised in-vivo flow and pressure data to tune 3EWM parameters achieved a good agreement with in-vivo measurements and has been widely accepted for CFD simulations in aortic dissection.

However, limited patient-specific data are available in most situations due to the lack of advanced imaging facilities or urgency in administrating treatment, resulting in no pressure and flow data for the purpose of parameter tuning. In this scenario, typically, only computed tomography (CT) scans and electrocardiogram (ECG) acquired during diagnosis are available. In CFD studies where patient-specific flow information is unavailable, a generic waveform from the literature is usually applied at the inlet, along with 3EWM parameters directly taken from previously published studies. As the absence of patient-specific flow data could result in non-patient-specific simulation results, <sup>19,26</sup> it would be desirable to personalise a generic flow waveform based on patient information that can be acquired during a standard clinical examination.

This study aims to develop a new tuning method to make the aortic inlet flow waveform more patient-specific in the absence of 4D-flow MRI. Specifically, ECG data (heart rate, and systolic and diastolic periods) and stroke volume (SV) are utilised to rescale a generic flow waveform. This workflow is evaluated through qualitative and quantitative analysis of simulation results for 5 type B aortic dissection (TABD) patients. 4D-flow MRI derived inlet boundary conditions are also used in patient-specific simulations to provide gold standard for comparison and validation.

## 2 | MATERIALS AND METHODS

## 2.1 | Data acquisition

The same patient data acquired as part of our previous study<sup>27</sup> were adopted here. Briefly, these included 5 TBAD patients (P1-P5) from Zhongshan Hospital, Fudan University, Shanghai. All patients received thoracic endovascular repair (TEVAR), and diagnostic ECG, CT and 4D-flow MRI were available. Patient-specific geometries were reconstructed from preoperative CT scans in Mimics (Materialise HQ, Leuven), and each model included all major side branches, including brachiocephalic (BRAC), left common carotid (LCCA) and left subclavian artery (LSA) from the aortic arch, celiac (CA), superior mesenteric artery (SMA), left and right renal (LR and RR) in the descending aorta, and left and right iliac artery (LIA and RIA) down to the aortic bifurcation. Reconstructed geometries are shown in Figure 1. Additionally, Doppler-wire pressure measurements were taken during TEVAR. This study compiled with the Declaration of Helsinki and was approved by the ethics committee of Zhongshan Hospital, Fudan University.

# 2.2 | Analysis of ECG waveform

ECG is a non-invasive procedure extensively utilised to evaluate the electrical activity of the heart over a specific period and was acquired for each patient during diagnosis. It records electrical signals generated by the cardiac muscle during each heartbeat. As shown in Figure 2, a typical ECG waveform consists of the P wave, QRS complex and T wave, which represent atrial depolarization, ventricular depolarization and repolarization, respectively. A cardiac period is represented by the time interval between two consecutive R waves, and a complete ventricular contraction activity is represented by the QRS-T interval. The ratio of cardiac systole and diastole period (SDR) was used to tune the inlet waveform for each patient, as discussed in Section 2.3, and was estimated as follows: first, a complete waveform was extracted from the ECG report using in-house MATLAB code; second, the extracted waveform was rescaled on the x-axis to match the actual cardiac period,  $T_{\rm cycle}$ ; finally, the contraction period was measured by the QRS-T interval. As a left ventricle contraction could end at any time within the T wave, an assumption was made that a complete contraction ended at the end of T wave for each patient. With this assumption, SDR could be estimated by QRS-T interval/ $T_{\rm cycle}$ -QRS-T interval). A total of 3 ECG waveforms were extracted for SDR calculation, and the average value from 3 different measurements was taken. Patient-specific information is summarised and shown in Table 1.

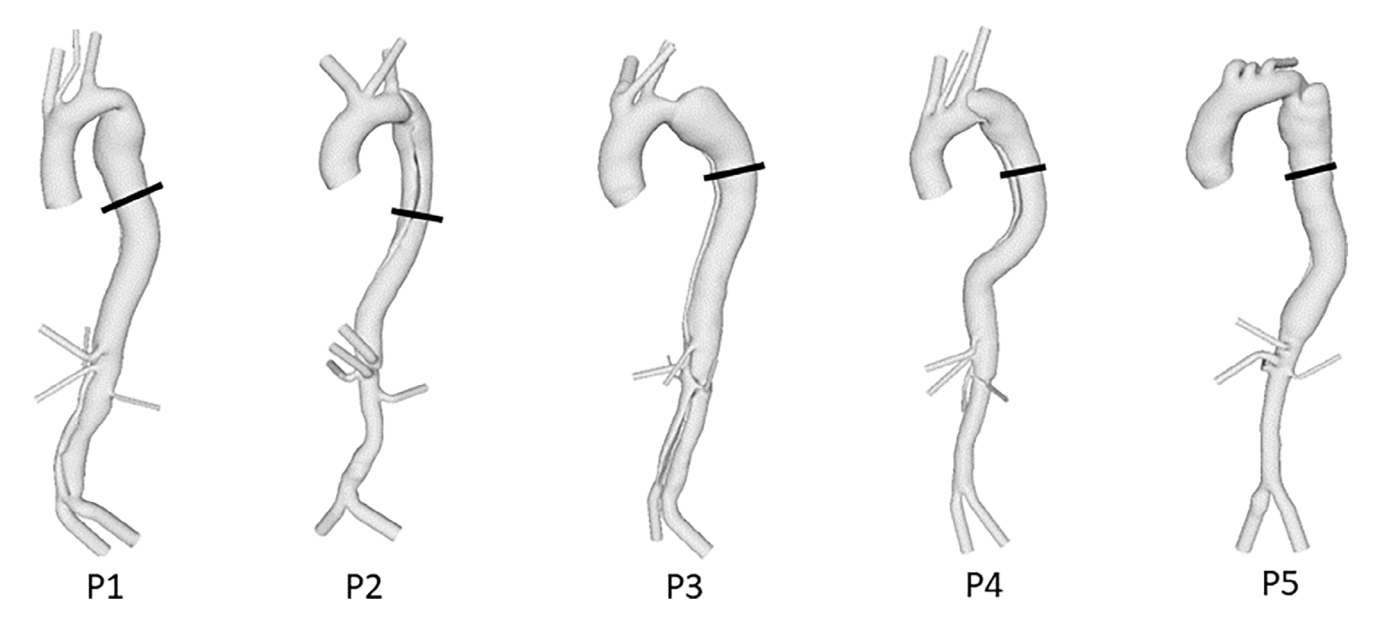


FIGURE 1 Reconstructed geometries of P1, P2, P3, P4 and P5; A plane, indicated on each model, was placed in the descending aorta for flow validations.

FIGURE 2 A typical representation of electrocardiogram waveforms and left ventricle output. QRS-T complex is correlated to contraction activities of the left ventricle. (A) Electrocardiogram and (B) left ventricle output.

**TABLE 1** Patient-specific information for patients P1–P5.

	Stroke volume (mL)	Cycle period (s)	SDR
P1	74	0.658	1.18
P2	116	1.048	1.15
P3	117	0.774	2.95
P4	117	0.942	1.58
P5	113	0.858	1.13

Note: SDR, ratio of cardiac systole and diastole period.

# 2.3 | Inlet flow waveform tuning

A generic flow waveform was adopted from the literature<sup>27</sup> and expressed using a Fourier series:

$$Q_{\text{generic}}(t) = A_0 + \sum_{i=0}^{\infty} A_i \cdot \cos(\omega_0 \cdot i \cdot t) + \sum_{i=0}^{\infty} (B_i \cdot \sin(\omega_0 \cdot i \cdot t)), \ t \in [0, T_{\text{cycle}}], \tag{1}$$

where Q is instantaneous flow rate,  $A_0$  is the average flow rate over one period,  $A_i$  and  $B_i$  are the Fourier coefficients to represent the oscillatory behaviour at the fundamental frequency  $\omega_0 = 2\pi/T_{\rm cycle}$ , where  $T_{\rm cycle}$  is the patient-specific cardiac period, and  $t \in T_{\rm cycle}$ . Figure 3 depicts the conversion of this generic waveform to the well-tuned waveform using P5 as an example.

First, the generic waveform was scaled to match the patient-specific  $T_{\rm cycle}$  (shown in blue in Figure 3A) which has a  $T_{\rm cycle}$  of 0.858 s with an SDR of 0.58. Based on the SDR derived from the ECG of P5 (Table 1), the durations of systole and diastole were 0.455 s and 0.403 s, respectively. This information was used to tune the waveform by varying the fundamental frequency as:

$$\omega_{0_{\text{new}}} = r * \omega_0, \tag{2}$$

where r is a frequency ratio calculated based on the systolic phase durations in both the generic and patient-specific waveforms. The widening of the systolic phase by setting r = 0.5 can be seen as an example in Figure 3A. The systole-matched waveform was then scaled to match the patient-specific SV by multiplying a factor defined as  $SV_{patient-specific}/SV_{systole-matched}$  as shown in Figure 3B. The final step was to perform a new Fourier transform on this well-tuned waveform within the same period  $t \in T_{cycle}$ , and this produced a periodic, patient-specific waveform.

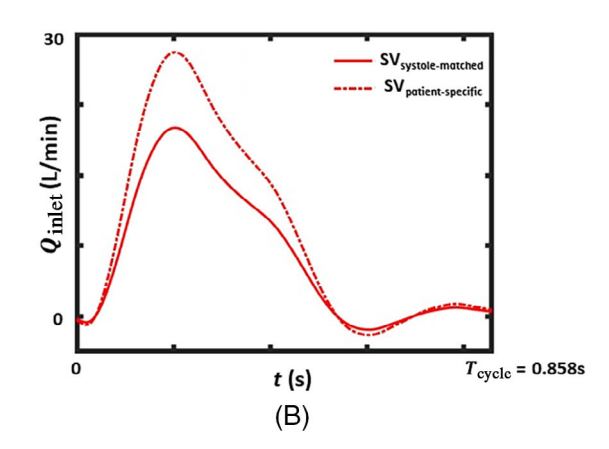


FIGURE 3 Patient-specific tuning process based on (A) the ratio of cardiac systole and diastole (SDR) and (B) stroke volume (SV).

In this study, all patients had a larger SDR compared with the generic waveform, therefore r < 1 was required to extend the systolic phase. However, if a patient had a smaller SDR, the diastolic phase would be extended by resampling the diastolic data over a longer period.

The process described above was implemented in our in-house Python code, which allows a user to automatically produce an inlet flow waveform based on their input values for SDR and SV for each patient.

## 2.4 | Outlet boundary conditions

3EWM was applied at all outlets for each geometry, with model parameters being calculated separately for each outlet using a simplified method. As reported in previous studies,  $^{25,27}$  the vasculature distal to the aortic geometry can be represented by a proximal resistance ( $R_1$ ), a compliance (C), and a distal resistance ( $R_2$ ). Without the need for patient-specific pressure measurements and flow splits into each outlet, which can be challenging to obtain, only the surface area of each outlet was required to calculate the 3EWM parameters. This was done by the following steps:

First, for each branch i, the total resistance,  $R_{t,i}$ , is adopted from the literature, <sup>27</sup> and  $C_i$  is calculated by:

$$C_i = \frac{\tau}{R_{t,i}},\tag{3}$$

where  $\tau$  has a constant value of 1.72.<sup>28</sup> After obtaining the area for each outlet,  $R_{1,i}$  is calculated using:

$$R_{1,i} = \frac{\rho c_i}{A_i},\tag{4}$$

$$c_i = \frac{a_2}{(2r_i)^{b_2}}, i = 1, 2, \dots,$$
 (5)

where  $\rho$  is the blood density,  $r_i$  is the radius of the outlet i,  $a_2$  and  $b_2$  are the empirical coefficients and equal to 13.3 and 0.3, <sup>29</sup> and n is the number of outlets. Finally,  $R_{2,i}$  is obtained by:

$$R_{2,i} = R_{t,i} - R_{1,i}, i = 1, 2, \dots n.$$
(6)

## 2.5 | Simulation setup

Reconstructed geometries were imported into ICEM (Ansys Inc., v19.0) and meshed with hexahedral core elements and 10 prism boundary layers. The mesh was refined in regions of tears and small branches. Mesh sensitivity tests were carried out to ensure mesh-independent results, and details can be found in our previous work.<sup>27</sup> A final mesh was



**TABLE 2** Three different sets of boundary conditions applied in each geometry.

Boundary condition name	Inlet boundary condition	Outlet boundary condition
4DMRI	Patient-specific time-varying 3D velocity profiles extracted from 4D-flow MRI	3EWM: Completely tuned based on measured flow and pressure
ECG + SV	Generic waveform tuned using patient-specific ECG and SV, flat velocity profile	3EWM: Simplified tuning based on outlet area
SV	Generic waveform tuned using patient-specific SV, flat velocity profile	3EWM: Simplified tuning based on outlet area

Abbreviations: 3EWM, 3-element Windkessel model; 4DMRI, 4D-flow magnetic resonance imaging; ECG, electrocardiogram; SDR, ratio of cardiac systole and diastole; SV, stroke volume.

selected to ensure <5% differences in mean and maximum velocity and time-averaged wall shear stress (TAWSS) comparing to a finer mesh, and 4–5 million elements were finally adopted for each patient depending on their geometry complexity.

Three simulations were performed for each patient, each with a different set of boundary conditions as summarised in Table 2. For the 4DMRI set, 4D-flow MRI data were processed using in-house Python codes to extract 3D time-varying inlet velocity profiles, just distal to the aortic valve, for each patient following our previously published methodology<sup>19,30</sup>—the python codes are available on Github.<sup>30</sup> Additionally, SV was measured from 4D-flow MRI for tuning purposes as described in Section 2.2. For the ECG + SV set, a well-tuned inlet waveform was generated following the method described in Section 2.2, and flat velocity profiles were assumed at the inlet. For the SV-based simulations, the same generic waveform was tuned to only match the SV following the aforementioned methodology (Figure 3B). All inlet waveforms adopted for each patient are shown in Figure 4. At outlets, patient-specific flow and pressure were used to tune 3EWM parameters for the 4DMRI set, and simplified tuning was applied for both the ECG + SV and SV sets following the method described in Section 2.3. A comprehensive list of all model parameters is presented in the Data S1.

CFD simulations were run with each set of boundary conditions for all five patients in Ansys CFX (Ansys Inc., 2022 R2). A total of 5 cardiac cycles with a timestep of 0.001 s were simulated to ensure that periodic results were achieved, and the final cycle was utilised for analysis. The Quemada non-Newtonian model was adopted to account for blood shear-thinning properties at high shear rates, <sup>31</sup> and its parameters were taken from the literature. <sup>12</sup> Qualitative and quantitative assessments were conducted on WSS-related metrics, flow patterns and pressure. WSS-related metrics were calculated and compared among different sets of boundary conditions. Flow validation was conducted by placing a plane (Figure 1) in the descending aorta where several flow features were measured and compared. These included retrograde flow fraction (RFF) and FL systolic antegrade flow fraction (FL<sub>SA</sub>) as defined in Equations (7) and (8), and false lumen ejection fraction (FLEF) (defined in Equation (9)) at the primary entry tear (PET). <sup>17</sup> Relative aortic pressure changes from the aortic root to the distal FL were computed and normalised by the aortic length.

$$Retrograde flow fraction (RFF) = \frac{Retrograde flow}{Retrograde flow + Antegrade flow} * 100\%, \tag{7}$$

False lumen systolic antegrade flow fraction  $(FL_{SA})$  =

$$\frac{\text{False lumen systolic antegrade flow}}{\text{False lumen systolic antegrade flow} + \text{True lumen systolic antegrade flow}} * 100\%, \tag{8}$$

False lumen ejection fraction (FLEF) = 
$$\frac{\text{Retrograde flow}}{\text{Antegrade flow}} * 100\%. \tag{9}$$

## 3 | RESULTS

## 3.1 | Flow assessment

Figure 5 shows flow distributions on the selected plane for each set of boundary conditions at four different timepoints during a cardiac cycle for all patients. Results extracted from 4DMRI simulations were treated as the gold standard for

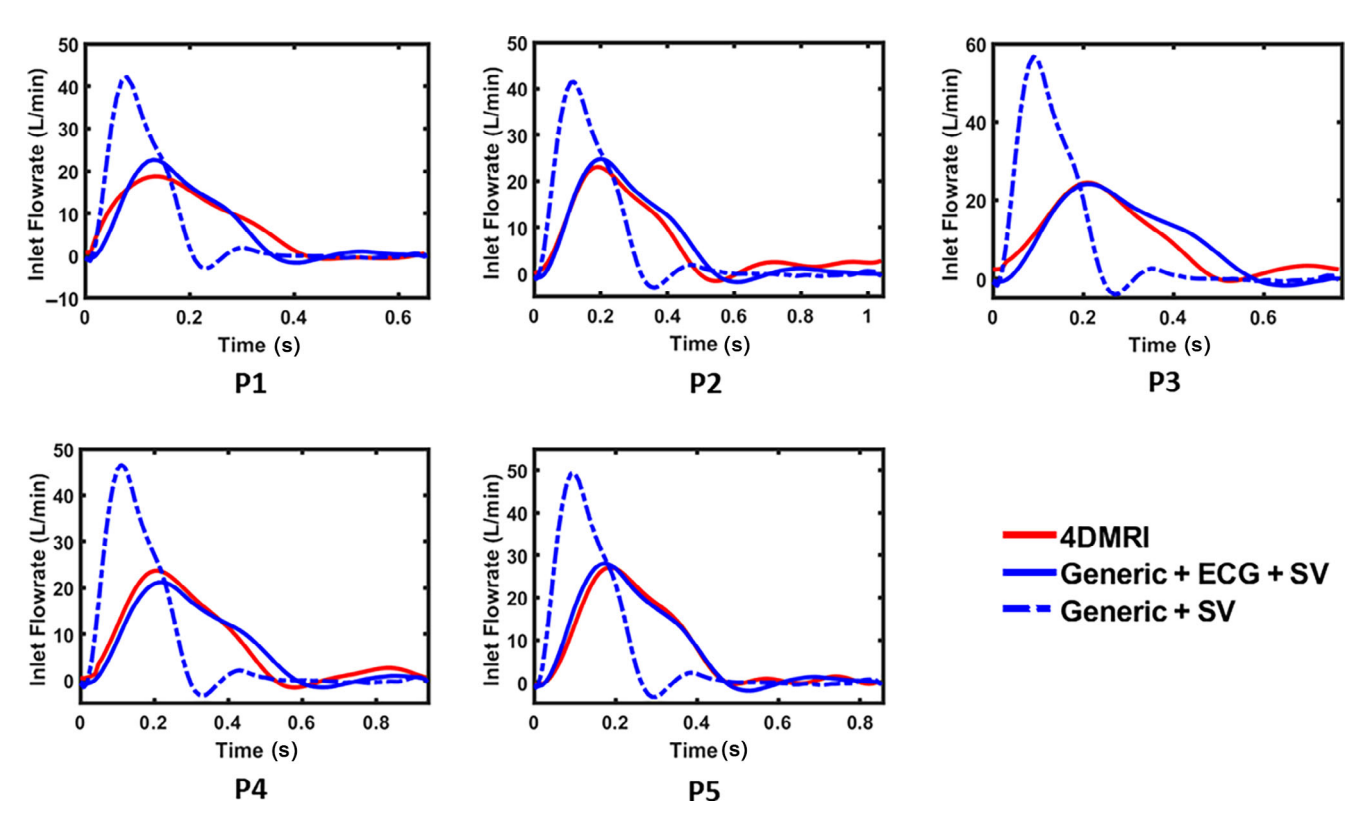


FIGURE 4 Different inlet waveforms for P1, P2, P3, P4 and P5. Red solid: Patient-specific waveforms extracted from 4D-flow MRI. Blue solid: Generic waveform tuned to match patient-specific stroke volume and ECG. Blue dashed: Generic waveform tuned to match patient-specific stroke volume.

comparison, and retrograde flows are shown in blue. ECG + SV-based simulations accurately reproduced the flow pattern in both the TL and FL throughout a cardiac cycle for all patients, whereas notable differences can be observed with the SV-based simulations. More specifically, SV-based simulations tended to overestimate flow in the FL, especially in P1, P3 and P5.

Net flow, defined as the total amount of flow passing through a given cross-section per unit time, was measured on the mid-thoracic plane in the descending aorta, and its variations throughout a cardiac cycle are shown in Figure 6. It can be seen that SV-based simulations had the poorest correlation with the 4DMRI gold standard results in all cases, with overestimated peak flowrates and shorter periods of reverse flow. In contrast, ECG + SV-based simulations not only captured very similar variations to the 4DMRI results throughout a cycle but also predicted more accurate peak flowrates than the SV results. Table 3 shows RRF and  $FL_{SA}$  measured on the mid-thoracic plane of each patient. Simulations with different sets of boundary conditions showed varying RFF across all five patients (P1–P5). 4DMRI simulation results presented a general trend of lower percentages from 1.1% to 15.0%, and ECG-SV based simulations resulted in slightly higher RFF predictions for each patient with RFF ranging from 4.1% to 16.0%. In contrast, SV-based simulations consistently overestimated RFF by a greater amount (from 8.0% to 21.2%). On the other hand, less difference was observed in  $FL_{SA}$  among the three simulation scenarios.

As shown in Figure 7, FLEF was calculated by placing a plane at the PET and measuring antegrade and retrograde flow volumes through this plane. Table 4 shows FLEF for each patient with different simulations. Low FLEF was accurately captured in P1, P3, P4 and P5 by ECG + SV-based simulations. In P2, a high FLEF of 51.3% was predicted by 4DMRI simulations, and this was accurately predicted by ECG + SV-based simulation, which predicted a value of 48.4%. In contrast, SV-based simulations overpredicted FLEF with a value ranging from 4.5% to 76.7%.

## 3.2 | Wall shear stress

Figure 8A shows TAWSS distribution for P1. Absolute difference contours relative to 4DMRI simulation results are also shown in Figure 8B. It is clear that ECG + SV-based simulations closely matched 4DMRI simulations in the descending

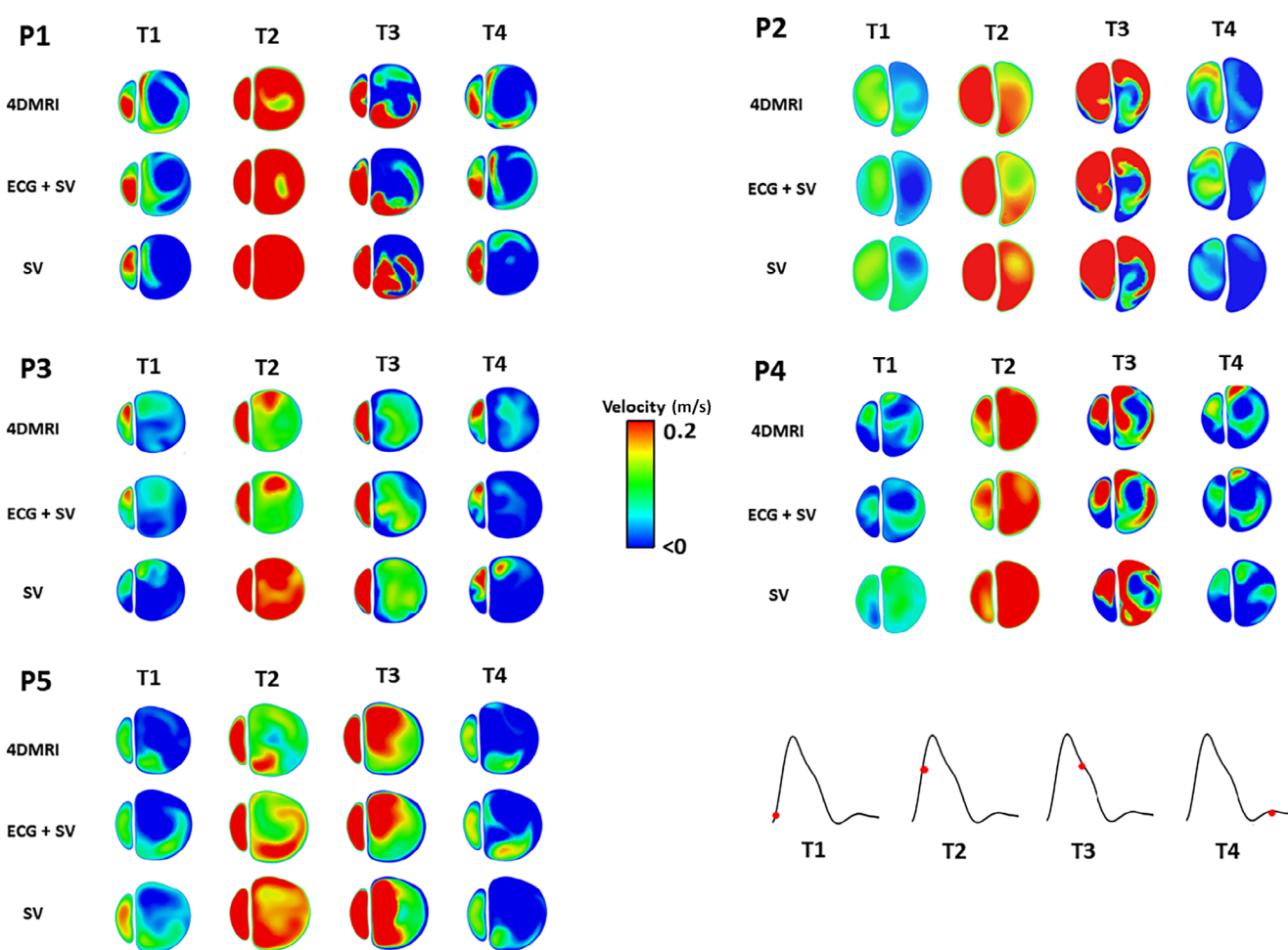


FIGURE 5 Flow distributions on the selected plane in the descending aorta for P1, P2, P3, P4 and P5 at early start, systolic acceleration, systolic deceleration and late diastole. Regions in blue indicate retrograde flows.

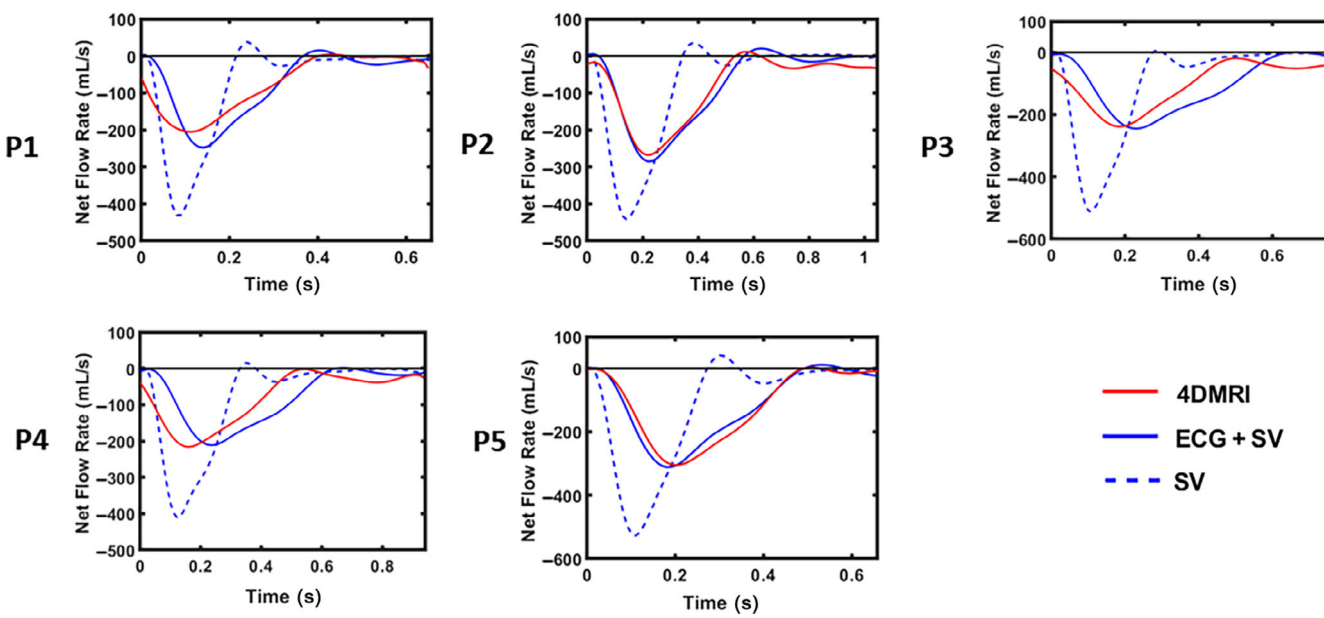


FIGURE 6 Variations of net flow on the selected plane in the descending aorta for P1, P2, P3, P4 and P5.

TABLE 3 Measurements of retrograde flow fraction and false lumen systolic antegrade flow fraction.

	Retrograde	Retrograde flow fraction (RFF)			False lumen systolic antegrade flow fraction ( $FL_{SA}$ )			
	4DMRI	ECG + SV	SV	4DMRI	ECG + SV	SV		
P1	10.8%	11.7%	18.8%	68.9%	64.3%	64.8%		
P2	7.6%	11.3%	17.5%	36.3%	33.0%	34.7%		
P3	1.1%	4.1%	8.0%	64.8%	61.0%	65.5%		
P4	6.2%	7.1%	11.6%	72.7%	72.4%	70.7%		
P5	15.0%	16.0%	21.2%	70.5%	71.5%	70.7%		

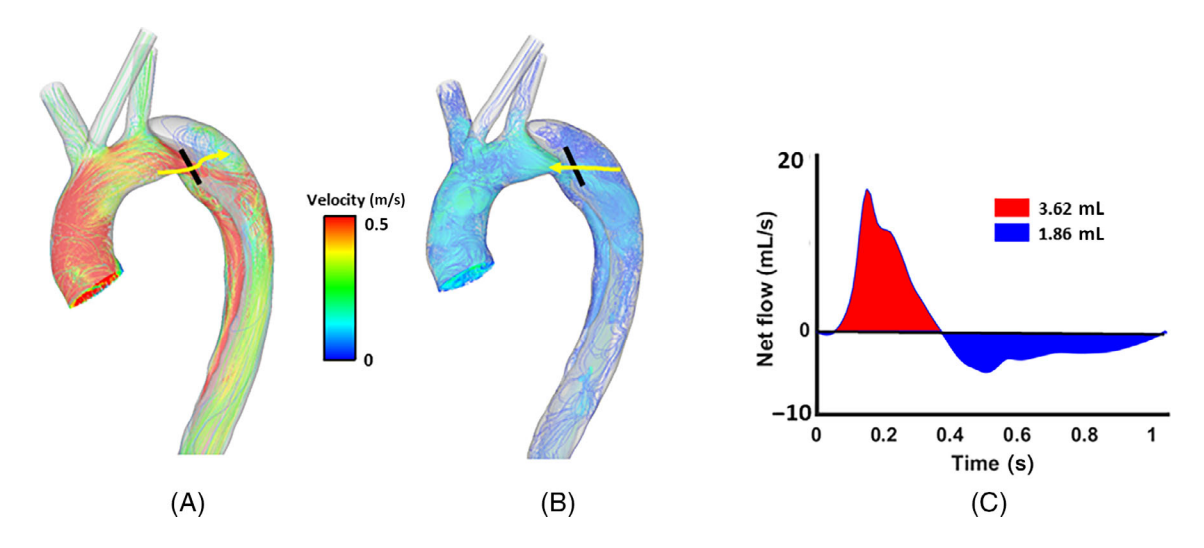


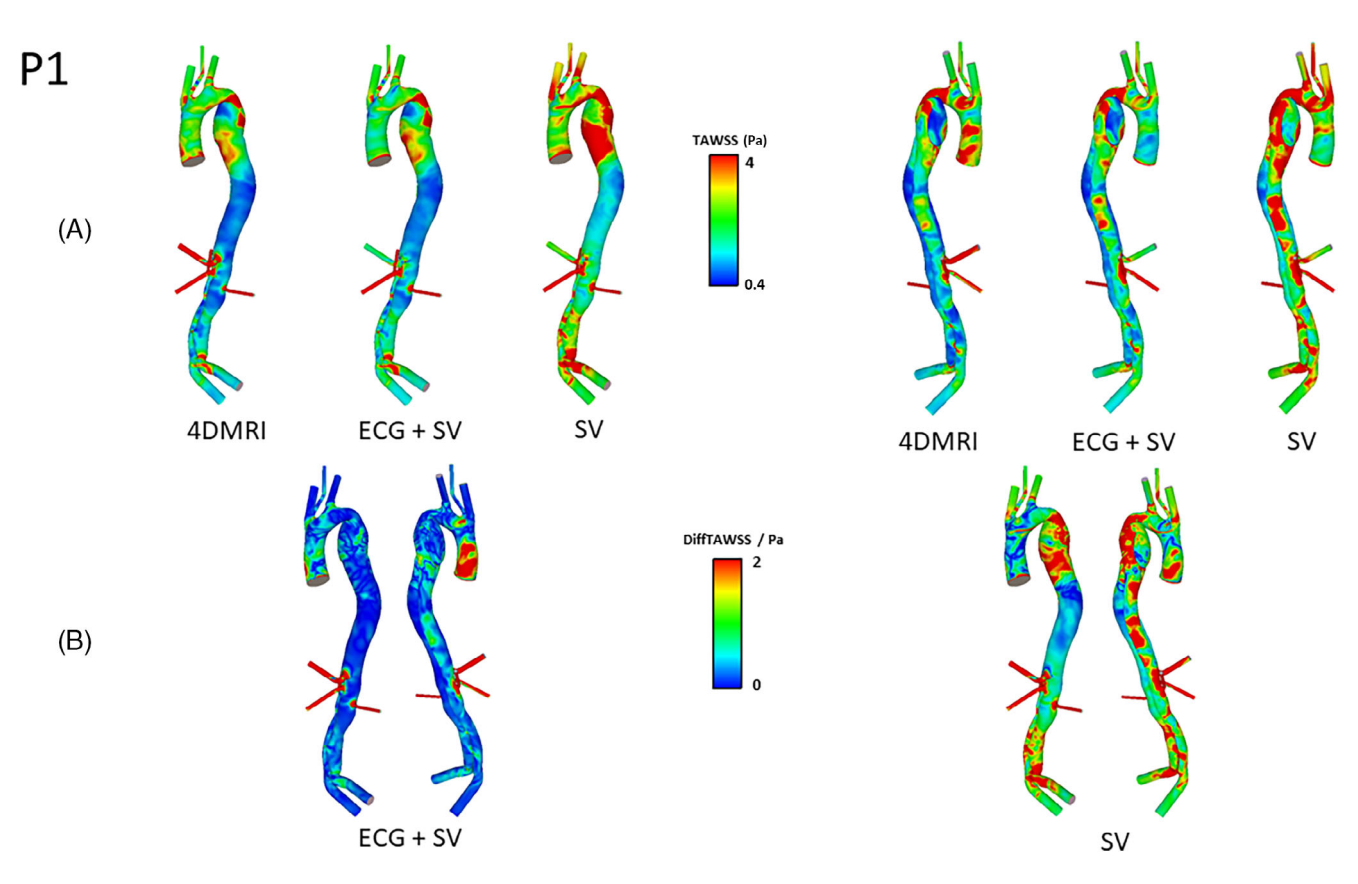
FIGURE 7 Measurements of antegrade flow (A) and retrograde flow (B). False lumen ejection fraction (FLEF) was calculated using volumes of antegrade and retrograde flow (C).

TABLE 4 Measurements of false lumen ejection fraction, %.

	4DMRI	ECG + SV	SV
P1	1.9%	1.7%	7.1%
P2	51.3%	48.4%	76.7%
P3	0.7%	3.8%	63.6%
P4	6.8%	6.7%	22.7%
P5	3.2%	3.0%	4.5%

aorta where both high and low TAWSS regions were captured precisely. However, notable differences can be observed in the SV-based simulation results with a much larger high TAWSS region near the PET and a smaller low TWASS zone in the abdominal region. In the ascending aorta (AAo), both ECG + SV-based and SV-based simulations failed to capture accurate TAWSS distributions. The same trends were observed in all other patients and detailed results can be found in Data S1.

Quantitative comparisons were made by evaluating mean and maximum TAWSS in different regions of the aorta. Table 5 shows mean TAWSS and its absolute difference compared with 4DMRI simulations in the AAo, PET and abdominal regions. In the AAo, ECG + SV-based simulations generally underestimated mean TAWSS for all patients with errors ranging from -35.2% to -50%, while SV-based simulations showed both underestimations and overestimations with errors ranging from -33.5% to 11.2%. In the PET and abdominal regions, ECG + SV-based simulations significantly reduced differences with a maximum difference of 15.0% in the PET and 22.8% in the abdominal region compared with 81.4% and 74.5% from SV-based simulations.



**FIGURE 8** (A) Time-averaged wall shear stress (TAWSS) distribution on P1 by 4DMRI, ECG + SV-based and SV-based simulations. (B) Absolute TAWSS difference compared with 4DMRI simulation.

**TABLE 5** Mean time-averaged wall shear stress (Pa) measurements.

Mear	n TAWSS (Pa)								
	AAo			PET			Abdominal		
	4DMRI	ECG + SV	SV	4DMRI	ECG + SV	SV	4DMRI	ECG + SV	SV
P1	3.04	1.92	2.69	2.61	2.76	4.29	1.34	1.52	2.22
P2	1.94	0.97	1.29	1.27	1.28	1.78	1.41	1.62	2.18
P3	1.79	1.16	1.99	1.13	1.3	2.05	1.27	1.56	2.21
P4	2.73	1.76	2.91	3.13	3.08	4.76	1.61	1.63	2.81
P5	2.36	1.37	2.09	1.35	1.28	1.79	1.27	1.23	1.75
Diffe	rence compai	ed with 4DMRI-	based simul	ation					
	4DMRI	ECG + SV	SV	4DMRI	ECG + SV	SV	4DMRI	ECG + SV	SV
P1	-	-36.8%	-11.5%	-	5.7%	64.4%	-	13.4%	65.7%
P2	-	-50.0%	-33.5%	-	0.8%	40.2%	-	14.9%	54.6%
P3	-	-35.2%	11.2%	-	15.0%	81.4%	-	22.8%	74.0%
P4	-	-35.5%	6.6%	-	-1.6%	52.1%	-	1.2%	74.5%
P5	-	-41.9%	-11.4%	-	-5.2%	32.6%	-	-3.1%	37.8%

Abbreviations: AAo, the ascending aorta; PET, the primary entry tear.

Table 6 shows the maximum TAWSS and its difference compared with 4DMRI simulations in the AAo, PET and abdominal region. The maximum TAWSS was observed on distal tears in all cases. Compared with 4DMRI simulations, ECG + SV-based simulations resulted in a maximum difference of -9.3% in the PET and 34.9% in the abdominal region excluding P3 who presented multiple distal tears in the abdominal region.

# 3.3 | Relative pressure difference

Figure 9 shows measurements of relative pressure difference between a plane placed at the aortic root and a plane placed in the descending FL. Pressure was measured on each plane, and relative aortic pressure difference,  $\Delta P$ , was computed over a cardiac cycle. As shown in Figure 9B, ECG + SV-based simulation captured the same variation of relative pressure difference throughout a cardiac cycle as the 4DMRI simulation in P2. Similar results were observed in other patients. For a quantitative comparison, the maximum pressure difference,  $\Delta P_{\rm max}$ , was measured for each simulation and the results are summarised in Table 7. It shows that ECG + SV-based simulations predicted close maximum pressure with an absolute difference ranging from 3.0% to 34.4%, while SV-based simulations greatly overpredicted this difference from 157.1% to 541.1%.

TABLE 6 Maximum time-averaged wall shear stress (Pa) measurements.

Maxi	mum TAWSS	S (Pa)								
	AAo			PET	PET			Abdominal		
	4DMRI	ECG + SV	SV	4DMRI	ECG + SV	SV	4DMRI	ECG + SV	SV	
P1	11.56	14.15	16.56	17.87	16.2	24.39	13.44	13.87	20.55	
P2	8.16	8.04	8.8	12.52	13.05	16.41	17.24	23.25	31.67	
Р3	16	12.08	13.74	7.02	7.97	9.69	16.32	29.42	27.65	
P4	10.23	14.82	19.01	33.77	34.8	45.55	21.02	22.82	33.16	
P5	13.45	12.65	13.95	14.87	14.22	17.15	7.6	7.13	10.39	
Diffe	rence compai	red with 4DMRI	-based simul	lation						
	4DMRI	ECG + SV	SV	4DMRI	ECG + SV	SV	4DMRI	ECG + SV	SV	
P1	-	22.4%	43.3%	-	-9.3%	36.5%	-	3.2%	52.9%	
P2	-	-1.5%	7.8%	-	4.2%	31.1%	-	34.9%	83.7%	
Р3	-	-24.5%	-89.1%	-	13.5%	38.0%	-	80.3%	69.4%	
P4	-	44.9%	85.8%	-	3.1%	34.9%	-	8.6%	57.8%	
P5	-	-5.9%	3.7%	-	-4.4%	15.3%	-	-6.2%	36.7%	

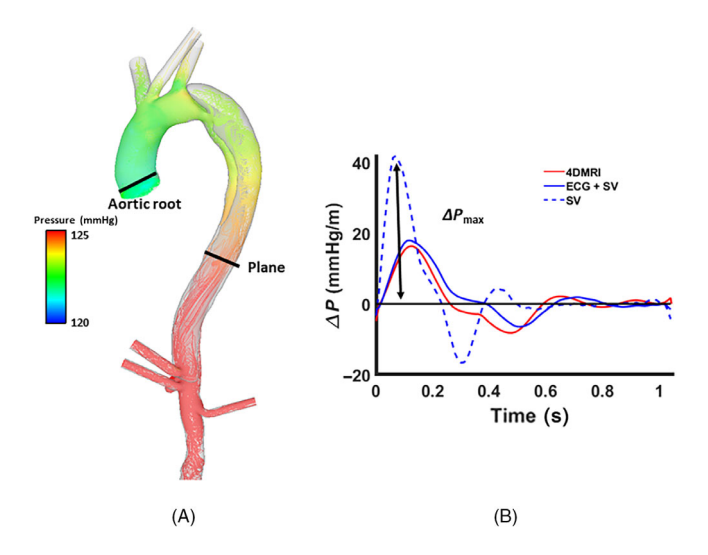


**FIGURE 9** (A) Relative pressure difference ( $\Delta P$ ) measurements from the aortic root to the false lumen in the descending aorta. (B) Variations of  $\Delta P$  predicted by 4DMRI, ECG + SV-based and SV-based simulations.



TABLE 7 Measurements of normalised maximum pressure difference,  $\Delta P_{\text{max}}$  (mmHg/m).

	4DMRI	ECG + SV (% difference)	SV (% difference)
P1	34.6	42.5 (22.8%)	124.8 (260.7%)
P2	16.3	17.9 (9.8%)	41.9 (157.1%)
P3	9.0	12.1 (34.4%)	57.7 (541.1%)
P4	20.2	19.6 (-3.0%)	68.6 (239.6%)
P5	24.1	27.5 (14.1%)	76.4 (217.9%)

## 4 | DISCUSSION

The role of hemodynamic metrics has been widely investigated in diagnosing cardiovascular diseases and predicting disease progression in recent years, <sup>7,9,10,14,17,32–34</sup> and CFD simulations have shown a great potential in assisting clinicians in risk stratification and treatment planning. In TBAD patients, high retrograde flow in the FL has been found to correlate with aortic growth and other unfavourable outcomes in the descending aorta. <sup>16,17</sup> Moreover, high WSS at the distal end of the implanted graft after TEVAR was found to be a risk factor for the formation of SINE, <sup>4</sup> and consistent high WSS on the surface of formed SINEs was related to rapid expansion. <sup>6</sup> Patient-specific boundary conditions derived from 4D-flow MRI and in-vivo pressure measurements have been shown to be critical to obtaining accurate simulation results. Inclusion of 3D spatial information at inlets can greatly improve accuracy in WSS distributions in the AAo, <sup>19</sup> and a well-tuned 3EWM model at all outlets helps to obtain more physiologically accurate flow and pressure data. <sup>25</sup>

However, patient-specific information is limited for most patients, resulting in the use of generic boundary conditions and hence less reliable predictions from CFD simulations. The most accepted and widely used tuning method for inlet flow waveforms is to scale a generic waveform to match patient-specific SV and cardiac period, but this can still result in significant differences compared with patient-specific simulations. <sup>18–20</sup> In this study, we proposed a new workflow for scaling the inlet waveform based on ECG data, to generate a new waveform that matches the patient-specific cardiac systole to diastole ratio (SDR), in addition to SV and cardiac period. ECG is usually acquired during clinical examinations for aortic dissection patients, while SV can be estimated from echocardiography data. At model outlets, a simplified method which only utilised cross-sectional area for tuning at each outlet was applied. The workflow was implemented, evaluated, and validated in 5 TBAD patients, and results obtained from ECG + SV-based simulations were quantitatively and qualitatively compared with results from both 4DMRI and SV-based simulations.

The results of the present study show, for the first time, that flow distribution in the mid-thoracic aorta estimated by ECG + SV-based simulation correlates extremely well with 4DMRI simulations in regions of retrograde and high-velocity flows. The consistency in SDR significantly reduced RFF difference from 74.1%, 130.3%, 87.1% and 41.3% (SV-based vs. 4DMRI) to 8.3%, 48.7%, 14.5% and 6.7% (ECG + SV-based vs. 4DMRI) for P1, P2, P4 and P5, respectively. In P3, low RFF was captured by both ECG + SV (4.1%) and 4DMRI (1.1%) based simulations due to an extremely short period of the cardiac diastole with a SDR value of 2.95. In contrast, the SV-based simulation overpredicted RFF with a value of 8.0%.

In addition, retrograde flow in the FL was further quantified by FLEF, the ratio of retrograde and antegrade flow through the PET, which has been suggested as a predictor of aortic growth.  $^{15,17}$  ECG + SV-based simulations also helped improved the accuracy of FLEF prediction by reducing the average difference from 149.1% (SV-based vs. 4DMRI) to 6.2% (ECG + SV-based vs. 4DMRI) excluding P3 who had a very low FLEF of .7%. Given that high FLEF is thought to indicate FL expansion, as suggested in comparative studies based on 4D-flow measurements,  $^{15,17}$  P2 (with an FLEF of 51%) is likely at high risk of rapid FL expansion, and additional treatment should be recommended. The important role of retrograde flows in predicting disease progression has been demonstrated in several studies,  $^{6,16,17,35}$  and while flows can be relatively easily measured directly from 4D-flow MRI, such data are often not available due to cost and required expertise. However, our new ECG + SV-based workflow presented here (which can be built from readily available clinical images and data) can greatly enhance the confidence of using CFD to evaluate retrograde flow in the FL.

It was suggested by Marlevi et al. <sup>17</sup> that the maximum relative pressure difference in the FL,  $\Delta P_{\rm max}$ , was a predictor of aortic growth, with low  $\Delta P_{\rm max}$  indicating higher risk of rapid expansion. ECG + SV-based simulations accurately predicted  $\Delta P_{\rm max}$  in the FL with an average difference of 16.8% versus 4DMRI simulations, while SV-based simulations induced significant errors with an average difference of 283.1% versus 4DMRI simulations. The lowest  $\Delta P_{\rm max}$  was

observed in P3 which would indicate a high risk of expansion based on the pressure difference criterion, <sup>17</sup> yet P3 had a low FLEF of .7% which indicates a low risk of expansion. <sup>15,17</sup> This result highlights a limitation of the current literature which has primarily utilised small sample sizes—more cases are needed to validate the role of FLEF and  $\Delta P_{\text{max}}$  in predicting aortic growth.

Inlet and outlet boundary conditions are known to significantly affect WSS distributions in both the AAo and PET regions. Our study shows that the SV-based inlet waveform, which was tuned to only match patient-specific SV, is unable to predict accurate WSS magnitudes and distributions in all cases, with an average TAWSS difference of 54.1% in the AAo and 61.3% in the abdominal region versus 4DMRI simulations. With ECG + SV-based simulations, the average TAWSS difference has been reduced to 5.7% in the PET and 11.1% in the abdominal. In addition, maximum TAWSS was also accurately predicted by ECG + SV-based simulations in all cases. At the PET, ECG + SV-based simulations accurately predicted maximum TAWSS, with a maximum difference of 13.5% versus 4DMRI simulations. In abdominal regions, both ECG + SV-based and SV-based simulations presented large differences in P3 compared with 4DMRI simulations. These differences may be caused by the presence of multiple small tears in the descending aorta, which lead to more disturbed flows in this region.

In the AAo, the absence of 3D spatial information results in no accurate predictions of TAWSS by both ECG + SV-based and SV-based tuning methods. The mean difference in TAWSS between ECG + SV-based and 4DMRI simulations was up to 40% in the AAo. No reliable results can be obtained from generic-scaled boundary conditions if the region of interest is the AAo. Using a parabolic IVP may produce AAo hemodynamics closer to those of the 4DMRI, however this would still be an idealised profile that lacks the asymmetric features resulting from the aortic valve leaflet motion. <sup>36,37</sup> To overcome this limitation, a recent study by Saitta et al. <sup>30</sup> presented a data-driven method to generate synthetic 3D inlet velocity profiles utilising principal component analysis and statistical shape modelling. This innovative method may help improve accuracy in the AAo and further enhance the reliability of CFD predictions. However, Mariotti et al. <sup>21</sup> showed that hemodynamic results were also affected by the spatial velocity distributions in 3D inlet profiles. The ratio between the upper and lower base of the truncated cone shaped velocity jet through the aortic valve was found to greatly affect WSS and velocity distributions in the AAo. The effects of synthetic 3D inlet velocity profiles are still unclear, and more validation work is needed. In future work, generation of synthetic 3D profiles will be carried out, and the difference between synthetic and patient-specific 3D inlet profiles will be compared.

Finally, the cardiac period, represented by R–R interval in the ECG waveform depicted in Figure 2, can be influenced by several factors, for example physical and mental activities, medication and stress level. Given that the ECG and 4D-flow MRI were acquired at different times for the patients included in this retrospective study, the cardiac period measured from 4D-flow MRI was used to rescale the ECG waveforms to ensure that all three sets of boundary conditions for each patient had the same cardiac period. The average SDR, measured from 3 different ECG waveforms for each patient, was then adopted to tune the inlet waveform. While the total cardiac period can be read directly from an ECG report, the reported value is an average measured over a certain time period during an ECG test, thus may not match the exact period of a single waveform. In addition, SV used in our workflow was measured from 4D-flow MRI for tuning purposes. In practical applications, SV should be estimated from other available data, such as echocardiography (which was not available for the patients in this study). While the assumptions of cardiac period and SV in ECG + SV-based and SV-based simulations might be positively biased toward 4DMRI-based simulations, our results emphasised the importance of SDR in shaping an inlet flow waveform and allowed us to appropriately draw comparative conclusion between the simulation workflows. Ideally, all patient-specific parameters should be derived from scans taken on the same day under the same conditions in future applications.

## 5 | CONCLUSION

This study proposed an ECG + SV-based method for scaling the inlet flow waveform for CFD simulations in aortic dissection, as well as a simplified method for tunning outlet 3EWM parameters. When compared with gold-standard 4D-flow MRI based simulations, the new ECG + SV-based workflow not only successfully captured accurate flow distributions in the descending aorta but also accurately predicted TAWSS magnitudes and distributions in the PET and abdominal regions. Although tested on TBAD geometries, the proposed method can be used to tailor inlet flow waveform needed in other aortic flow simulations, such as thoracic or abdominal aortic aneurysms. This will allow the simulation results to be more patient-specific and greatly enhance the confidence of hemodynamic simulations in clinical applications when 4D-flow MRI is not available.



## 5.1 | Limitation

In this study, the aortic wall and intimal flap were assumed to be rigid in all simulations. As previous studies have demonstrated that mobile flaps and moving walls have a significant impact on both magnitude and distribution of low WSS,  $^{38,39}$  this assumption would affect TAWSS distributions in each case. However, considering this study was designed to compare and validate ECG + SV-based and SV-based simulations with 4DMRI simulations, the consistency of a rigid wall assumption in all cases allows for comparative conclusions to be drawn.

#### **AUTHOR CONTRIBUTIONS**

KW: Formal analysis; methodology; visualisation; writing. CHA: Supervision; review & editing; validation. BG: Data curation; review & editing. XYX: Conceptualization; supervision; review & editing.

#### FUNDING INFORMATION

This research was supported by the National Natural Science Foundation of China (grant number: 81770508), the Natural Science Foundation Project of Fujian Province (2023J011687), the Science and Technology Commission of Shanghai Municipality (21410710500), the Shanghai Municipal Health Commission's Health Youth Talent Training Program (2022YQ13), the Clinical Medicine Innovation Fund of Fudan Zhangjiang Institute (KP7202116), and the Royal Society, UK (grant number: IE161052). CHA is supported by the Imperial College London BHF Centre of Research Excellence (grant number: RE/18/4/34215).

#### CONFLICT OF INTEREST STATEMENT

The authors declare no conflict of interest.

#### DATA AVAILABILITY STATEMENT

The data that support the findings of this study are available on request from the corresponding author. The data are not publicly available due to privacy or ethical restrictions.

#### ORCID

*Xiao Yun Xu* https://orcid.org/0000-0002-8267-621X

## REFERENCES

- Cheng Z, Wood NB, Gibbs RG, Xu XY. Geometric and flow features of type B aortic dissection: initial findings and comparison of medically treated and stented cases. Ann Biomed Eng. 2015;43:177-189.
- 2. Cheng Z, Riga C, Chan J, et al. Initial findings and potential applicability of computational simulation of the aorta in acute type B dissection. *J Vasc Surg.* 2013;57(2):35S-43S.
- 3. Zhu Y, Zhan W, Hamady M, Xu XY. A pilot study of aortic hemodynamics before and after thoracic endovascular repair with a double-branched endograft. *Med Novel Technol Dev.* 2019;4:100027.
- 4. Menichini C, Pirola S, Guo B, Fu W, Dong Z, Xu XY. High wall stress may predict the formation of stent-graft–induced new entries after thoracic endovascular aortic repair. *J Endovasc Ther*. 2018;25(5):571-577.
- 5. Qiao Y, Luan J, Mao L, Fan J, Zhu T, Luo K. Biomechanical mechanism of distal stent-graft-induced new entry deterioration after thoracic endovascular aortic repair. *Phys Fluids*. 2022;34:101902.
- 6. Wang K, Armour CH, Ma T, Dong Z, Xu XY. Hemodynamic parameters impact the stability of distal stent graft-induced new entry. *Sci Rep.* 2023;13(1):12123.
- 7. Kumar VS, Kumar VS. High wall shear incites cerebral aneurysm formation and low wall shear stress propagates cerebral aneurysm growth. *J Neurol Res.* 2023;13(1):1-11.
- 8. Pavlin-Premrl D, Boopathy SR, Nemes A, et al. Computational fluid dynamics in intracranial atherosclerosis-lessons from cardiology: a review of CFD in intracranial atherosclerosis. *J Stroke Cerebrovasc Dis.* 2021;30(10):106009.
- 9. Alimohamadi M, Pichardo-Almarza C, Di Tomaso G, Balabani S, Agu O, Diaz-Zuccarini V. Predicting atherosclerotic plaque location in an iliac bifurcation using a hybrid CFD/biomechanical approach. *Bioinformatics and Biomedical Engineering: Third International Conference, IWBBIO 2015, Granada, Spain, April 15-17, 2015 Proceedings, Part II 3.* Springer; 2015.
- 10. Krams R, Wentzel J, Oomen J, et al. Evaluation of endothelial shear stress and 3D geometry as factors determining the development of atherosclerosis and remodeling in human coronary arteries in vivo: combining 3D reconstruction from angiography and IVUS (ANGUS) with computational fluid dynamics. *Arterioscler Thromb Vasc Biol.* 1997;17(10):2061-2065.

- Taylor JO, Meyer RS, Deutsch S, Manning KB. Development of a computational model for macroscopic predictions of device-induced thrombosis. Biomech Model Mechanobiol. 2016;15(6):1713-1731.
- 12. Menichini C, Xu XY. Mathematical modeling of thrombus formation in idealized models of aortic dissection: initial findings and potential applications. *J Math Biol.* 2016;73(5):1205-1226.
- 13. Yang L, Neuberger T, Manning KB. In vitro real-time magnetic resonance imaging for quantification of thrombosis. *MAGMA*. 2021;34 (2):285-295.
- 14. Wang K, Armour CH, Gibbs RG, Xu XY. A numerical study of the effect of thrombus breakdown on predicted thrombus formation and growth. *Biomech Model Mechanobiol.* 2023;1-11:61-71.
- 15. Burris NS, Nordsletten DA, Sotelo JA, et al. False lumen ejection fraction predicts growth in type B aortic dissection: preliminary results. *Eur J Cardiothorac Surg.* 2020;57(5):896-903.
- 16. Evangelista A, Pineda V, Guala A, et al. False lumen flow assessment by magnetic resonance imaging and long-term outcomes in uncomplicated aortic dissection. *J Am Coll Cardiol*. 2022;79(24):2415-2427.
- 17. Marlevi D, Sotelo JA, Grogan-Kaylor R, et al. False lumen pressure estimation in type B aortic dissection using 4D flow cardiovascular magnetic resonance: comparisons with aortic growth. *J Cardiovasc Magn Reson.* 2021;23(1):51.
- 18. Tajeddini F, Romero DA, McClarty D, Chung J, Amon C. Workflow comparison for combined 4D MRI/CFD patient-specific cardiovascular flow simulations of the thoracic aorta. *J Fluids Eng.* 2023;145(6):061106.
- 19. Armour CH, Guo B, Pirola S, et al. The influence of inlet velocity profile on predicted flow in type B aortic dissection. *Biomech Model Mechanobiol*. 2021;20(2):481-490.
- Stokes C, Ahmed D, Lind N, et al. Aneurysmal growth in type-B aortic dissection: assessing the impact of patient-specific inlet conditions on key haemodynamic indices. J R Soc Interface. 2023;20(206):20230281.
- 21. Mariotti A, Celi S, Antonuccio MN, Salvetti MV. Impact of the spatial velocity inlet distribution on the hemodynamics of the thoracic aorta. *Cardiovasc Eng Technol.* 2023;14(5):713-725.
- 22. Kim HJ, Vignon-Clementel I, Coogan J, Figueroa C, Jansen K, Taylor C. Patient-specific modeling of blood flow and pressure in human coronary arteries. *Ann Biomed Eng.* 2010;38:3195-3209.
- 23. Mousavi SJ, Jayendiran R, Farzaneh S, et al. Coupling hemodynamics with mechanobiology in patient-specific computational models of ascending thoracic aortic aneurysms. *Comput Methods Programs Biomed.* 2021;205:106107.
- 24. Munshi B, Parker LP, Norman PE, Doyle BJ. The application of computational modeling for risk prediction in type B aortic dissection. *J Vasc Surg.* 2020;71(5):1789-1801. e3.
- 25. Pirola S, Cheng Z, Jarral O, et al. On the choice of outlet boundary conditions for patient-specific analysis of aortic flow using computational fluid dynamics. *J Biomech.* 2017;60:15-21.
- 26. Tricarico R, Berceli SA, Tran-Son-Tay R, He Y. Non-invasive estimation of the parameters of a three-element windkessel model of aortic arch arteries in patients undergoing thoracic endovascular aortic repair. *Front Bioeng Biotechnol.* 2023;11:1127855.
- 27. Armour CH, Guo B, Saitta S, et al. Evaluation and verification of patient-specific modelling of type B aortic dissection. *Comput Biol Med.* 2021;140:105053.
- 28. Xiao N, Alastruey J, Alberto FC. A systematic comparison between 1-D and 3-D hemodynamics in compliant arterial models. *Int J Numer Methods Biomed Eng.* 2014;30(2):204-231.
- 29. Reymond P, Merenda F, Perren F, Rufenacht D, Stergiopulos N. Validation of a one-dimensional model of the systemic arterial tree. *Am J Physiol.* 2009;297(1):H208-H222.
- 30. Saitta S, Maga L, Armour C, et al. Data-driven generation of 4D velocity profiles in the aneurysmal ascending aorta. *Comput Methods Programs Biomed*. 2022;233:107468.
- 31. Quemada D. Rheology of concentrated disperse systems II. A model for non-newtonian shear viscosity in steady flows. *Rheol Acta*. 1978; 17(6):632-642.
- 32. Qiao Y, Mao L, Wang Y, Luan J, Ding Y, Zhu T. Fluid structure interaction: insights into biomechanical implications of endograft after thoracic endovascular aortic repair. *Comput Biol Med.* 2021;138:104882.
- 33. Wang H, Uhlmann K, Vedula V, Balzani D, Varnik F. Fluid-structure interaction simulation of tissue degradation and its effects on intra-aneurysm hemodynamics. *Biomech Model Mechanobiol.* 2022;21(2):671-683.
- 34. Kan X, Ma T, Lin J, Wang L, Dong Z, Xu XY. Patient-specific simulation of stent-graft deployment in type B aortic dissection: model development and validation. *Biomech Model Mechanobiol.* 2021;20(6):2247-2258.
- 35. Burris NS, Fleischmann D, Hope MD. Blood flow patterns of risk in aortic dissection: time to go with the flow? *J Am Coll Cardiol*. 2022; 79:2428-2430.
- 36. Qiao Y, Mao L, Wang Y, et al. Hemodynamic effects of stent-graft introducer sheath during thoracic endovascular aortic repair. *Biomech Model Mechanobiol*. 2022;21(2):419-431.
- 37. Youssefi P, Gomez A, Arthurs C, Sharma R, Jahangiri M, Alberto FC. Impact of patient-specific inflow velocity profile on hemodynamics of the thoracic aorta. *J Biomech Eng.* 2018;140(1):011002.
- 38. Chong MY, Gu B, Chan BT, Ong ZC, Xu XY, Lim E. Effect of intimal flap motion on flow in acute type B aortic dissection by using fluid-structure interaction. *Int J Numer Methods Biomed Eng.* 2020;36(12):e3399.
- 39. Qiao Y, Zeng Y, Ding Y, Fan J, Luo K, Zhu T. Numerical simulation of two-phase non-Newtonian blood flow with fluid-structure interaction in aortic dissection. *Comput Methods Biomech Biomed Engin*. 2019;22(6):620-630.

## SUPPORTING INFORMATION

Additional supporting information can be found online in the Supporting Information section at the end of this article.

**How to cite this article:** Wang K, Armour CH, Guo B, Dong Z, Xu XY. A new method for scaling inlet flow waveform in hemodynamic analysis of aortic dissection. *Int J Numer Meth Biomed Engng.* 2024;40(9):e3855. doi:10.1002/cnm.3855